Low energy electron-impact ionization of hydrogen atom for coplanar equal-energy-sharing kinematics in Debye plasmas

Jun Li, Song Bin Zhang, Bang Jiao Ye, Jian Guo Wang, and R. K. Janev

Citation: Phys. Plasmas **23**, 123511 (2016); doi: 10.1063/1.4971451
View online: http://dx.doi.org/10.1063/1.4971451
View Table of Contents: http://aip.scitation.org/toc/php/23/12
Published by the American Institute of Physics

Low energy electron-impact ionization of hydrogen atom for coplanar equal-energy-sharing kinematics in Debye plasmas

Jun Li,[1] Song Bin Zhang,[2,a)] Bang Jiao Ye,[1,b)] Jian Guo Wang,[3] and R. K. Janev[4]
[1]State Key Laboratory of Particle Detection and Electronics, Department of Modern Physics, University of Science and Technology of China, 230026 Hefei, People's Republic of China
[2]School of Physics and Information Technology, Shaanxi Normal University, 710119 Xian, China
[3]Key Laboratory of Computational Physics, Institute of Applied Physics and Computational Mathematics, P.O. Box 8009, Beijing 100088, China
[4]Macedonian Academy of Sciences and Arts, P.O. Box 428, 1000 Skopje, Macedonia

(Received 15 October 2016; accepted 22 November 2016; published online 15 December 2016)

Low energy electron-impact ionization of hydrogen atom in Debye plasmas has been investigated by employing the exterior complex scaling method. The interactions between the charged particles in the plasma have been represented by Debye-Hückel potentials. Triple differential cross sections (TDCS) in the coplanar equal-energy-sharing geometry at an incident energy of 15.6 eV for different screening lengths are reported. As the screening strength increases, TDCS change significantly. The evolutions of dominant typical peak structures of the TDCS are studied in detail for different screening lengths and for different coplanar equal-energy-sharing geometries. *Published by AIP Publishing.* [http://dx.doi.org/10.1063/1.4971451]

I. INTRODUCTION

As a result of the collective effects of correlated many-particle interactions, hot, dense plasmas exhibit screened Coulomb interactions.[1–3] The screened Coulomb interactions strongly affect the electronic structure (spectral) properties of atoms and the properties of their collision processes with respect to those for isolated systems.[4–7] Indeed, red-shifted spectral lines have been experimentally observed in a number of laser-produced dense plasmas;[8–12] these studies have inspired and promoted a large amount of theoretical investigations on the plasma screening effects on atomic excitation and ionization processes. The study of screened Coulomb interactions in plasma environments becomes one of the major subjects in plasma physics.[4–7,13–15]

In hot, dense plasmas, such as those created by laser irradiation of solids, and sometimes met also in the inertial confinement fusion research or in the stellar interiors, the potential energy is relatively small compared to the kinetic energy, long-range self-consistent interactions (described by the Poisson equation) dominate over short-range two-particle interactions (collisions), the pair-wise correlation approximation can be applied, and the screened Coulomb potential reduces to the well known Debye-Hückel potential.[15] For an ion of positive charge interacting with an electron, it is given by[1–5]

$$V(r) = -\frac{Ze^2}{r}\exp\left(-\frac{r}{D}\right), \tag{1}$$

where D is the plasma screening length, $D = \sqrt{k_B T_e/4\pi e^2 n_e}$, with k_B being the Boltzmann constant, T_e and n_e being the plasma electron temperature and density, respectively.

Due to its simple form and easy implementation in the calculations, Debye-Hückel potential has been broadly used in the theoretical studies of quantitative plasma screening effects on the atomic structures and collisions in hot, dense plasmas (Debye plasmas).[2–4,7,15] The most important properties of the screened Coulomb potential of Eq. (1) are that it lifts the Coulomb-degeneracy of energy levels of hydrogen-like systems and that for a given value of D, it supports only a finite number of bound states.[16] This implies that with decreasing the Debye length, the binding energies of states decrease and the energy levels successively enter into the continuum at certain critical screening lengths. For instance, the critical screening lengths for the $1s$, $2s$, and $2p$ states of hydrogen atom in a Debye plasma are 0.839907, 3.222559, and 4.540956 a.u., respectively.[17] Furthermore, with decreasing D, the excitation threshold energies also decreases, and the corresponding wave functions become increasingly more diffuse.[18] The atomic structures of hydrogen-like ions,[17,19] hydrogen negative ions,[20,21] helium,[22,23] helium-like ions,[24,25] positronium negative ion,[26–28] and many-electron systems[29–31] have also been systematically studied in Debye plasmas with the potential (1). Note that the structures of hydrogen atom and hydrogen molecule ion in both Debye potentials and exponential cosine screened Coulomb potentials have also been studied.[32]

The plasma screening effects in the dynamics of atomic collision processes taking place in Debye plasmas has recently been comprehensively reviewed.[15] For the scatterings with hydrogen atom in Debye plasmas, Ghoshal *et al.*[33] studied the elastic electron scatterings and presented the phase shifts of the S-wave singlet state below hydrogen $n = 2$ excitation threshold. Zhang *et al.*[34–36] investigated the excitation dynamics of low-energy electron colliding with hydrogen near the $n = 2$ and $n = 3$ excitation thresholds by the R-matrix method with pseudostates.[37] They revealed the phenomenon of crossover of Feshbach resonances into

a)song-bin.zhang@snnu.edu.cn
b)bjye@ustc.edu.cn

shape-type resonances with varying the screening length, a phenomenon directly related to the lifting of the Coulomb degeneracy by the screened Coulomb potential. By using the convergent-close-coupling method,[38] Zammit *et al.*[39] have calculated the excitation and total ionization cross sections in electron-hydrogen atom collisions in Debye plasmas in the low and intermediate energy region (from threshold to several hundreds of eV). They found that as the strength of the screening increases, the excitation cross sections decrease, whereas the total ionization cross section increases. By using a plane-wave description of incident electron, Qi *et al.*[40] have calculated the generalized oscillator strengths (GOS) for the fast electron-hydrogen atom collision in a Debye plasma and found that the screened interaction reduces the generalized oscillator strengths for transitions between the states with different n and increases them between the states with the same n. They also calculated the single differential ionization cross sections (SDCS) of hydrogen-like ions for the geometry with a fast scattering electron and a slow ejected electron.[17,41] Abundant structures have been revealed in the GOS, related to the shape resonances in the effective potential.

In the present work, we shall investigate the triple differential cross sections (TDCS) of low-energy electron-impact ionization of hydrogen atom in Debye plasmas for coplanar equal-energy-sharing kinematics. The aim of our study is to provide information on the electron impact ionization of hydrogen atom in Debye plasmas in the kinematics with strongly correlated scattered and ejected electrons, and, more specifically to reveal the plasma screening effects on TDCS. It is demonstrated that the plasma screening of the Coulomb interaction between interacting particles introduces significant changes in the TDCS peak structures. The calculations are performed with the exterior complex scaling method[42–45] to fully account for the electron-electron correlations. A brief account of the method is given in Section II. The results of our calculations are presented and discussed in Section III, and the conclusions are given in Section IV. Atomic units (a.u.) are used throughout this work unless explicitly stated otherwise.

II. METHOD OF CALCULATIONS

The theory of the exterior complex scaling (ECS) method and its implementation for electron-hydrogen atom collisions have been discussed in details in many papers,[42–44] and it is not necessary to repeat its full description here. Within the theory of ECS for electron-hydrogen atom scattering, the total scattering wave functions $\psi^{LMS\Pi}_{l_1l_2}(r_1,r_2)$ are obtained by solving a set of bi-radial equations

$$(E-\hat{H}_1-\hat{H}_2)\psi^{LMS\Pi}_{l_1l_2}-\sum_{l_1'l_2'}\left\langle y^{LM}_{l_1l_2}|V_{12}|y^{LM}_{l_1'l_2'}\right\rangle\psi^{LMS\Pi}_{l_1'l_2'}=\chi^{LMS\Pi}_{l_1l_2}, \tag{2}$$

where E is the total energy of the three-body system, $\hat{H}_1$ or $\hat{H}_2$ is the single-electron Hamiltonian including the electron kinetic part and electron-proton interaction, V_{12} represents the electron-electron interaction, and $y^{LM}_{l_1l_2}$ is the bi-polar spherical function.[42–44] $\chi^{LMS\Pi}_{l_1l_2}$ is the initial wave function, which can be written as

$$\begin{aligned}\chi^{LMS\Pi}_{l_1l_2}(r_1,r_2)=&\frac{1}{k_i}\sum_l\sqrt{2\pi(2l+1)}C^{LM}_{l_im_il0}i^l\\&\times\left[\left(\langle l_1l_2||V_{12}||l_il\rangle_L-\frac{1}{r_2}\delta^{l_i}_{l_1}\delta^{l}_{l_2}\right)\right.\\&\left.\times P_{n_il_i}(r_1)\hat{j}_l(k_ir_2)+(-1)^{S+\Pi}(1\leftrightarrow 2)\right],\end{aligned} \tag{3}$$

where k_i is the projectile electron momentum, $C^{LM}_{l_im_il0}$ is the Clebsch-Gordan coefficient, L, M are the total angular quantum number and its projection (both conserved in the collision process), l_i is the angular quantum number of the initial hydrogen orbital, m_i is the pertinent magnetic quantum number, and l is the partial wave of the projectile electron. Without loss of generality, the projectile electron is chosen along the z direction so that $m=0$. $P_{n_il_i}(r_1)$ represents initial hydrogen orbital and $\hat{j}_l(k_ir_2)$ is the Ricatti-Bessel function representing the projectile electron. The last term in Eq. (3) represents the exchange effects between the projectile electron and the target electron; S and Π are the total spin and parity of the system, respectively.

Generally, Eq. (2) can be completely solved by matching the wave functions from an inner radial region with the boundary conditions.[44] Many methods are based on this idea (e.g., the R-matrix method,[46] the convergent close-coupling method,[47] etc). The ECS method attempts to avoid matching the solutions of the inner region with the sophisticated boundary conditions and makes a complex scaling of the real radial coordinates as

$$R(r)=\begin{cases}r & r<R_0\\ R_0+(r-R_0)e^{i\theta_{ECS}} & r>R_0,\end{cases} \tag{4}$$

where R_0 is the complex scaling turning point and θ_{ECS} is the complex scaling argument. In the complex region $r>R_0$, the outward scattering wave functions with complex scaling would be exponentially damped; if the complex region is sufficiently long, the scattering wave functions should be damped to zero. Thus, in the ECS method, the original sophisticated boundary conditions are substituted simply by zero. The exact scattering wave functions $\psi^{LMS\Pi}_{l_1l_2}$ in the $r<R_0$ region can be obtained, and the scattering and ionization variables can be extracted by projecting the scattering wave functions to the final states of the system.

In the scattering process, the scattering T-matrix T^{LS}_l can be calculated by projecting $\psi^{LMS\Pi}_{l_1l_2}$ to the continuum + bound compound state as

$$\begin{aligned}T^{LS}_l=&\frac{1}{\sqrt{2}}\frac{4\pi}{k_f}i^{-l}C^{Lm_i}_{l_fm_flm_i-m_f}\\&\times\lim_{R_0\to\infty}\int_0^{R_0}P_{n_fl_f}(r_1)W\left[\psi^{LMS}_{l_fl}(r_1,r_2),\hat{j}_l(k_fr_2)\right]_{R_0}dr_1,\end{aligned} \tag{5}$$

where k_f is the scattering electron momentum in the final state, $C^{Lm_i}_{l_fm_flm_i-m_f}$ is the Clebsch-Gordan coefficient, R_0 is the

complex scaling turning point, $P_{n_f l_f}$ is the hydrogen orbital for the final state, $W[a,b]_{R_0} = a'(R_0)b(R_0) - a(R_0)b'(R_0)$ is the Wronskian of the two functions, and $\hat{j}_l(k_f r_2)$ is the Ricatti-Bessel function representing the scattered electron. The integral cross sections (ICS) can be obtained from the T-matrix,[48] and the complete cross section (CCS) is the sum of ICS

$$\sigma_{fi}^{LS} = \frac{k_f}{k_i}\frac{2S+1}{4}\frac{1}{4\pi^2}\sum_{lL'} T_{fi,l}^{LS} T_{fi,l}^{L'S*}, \quad \sigma_{fi} = \sum_{LS}\sigma_{fi}^{LS}. \tag{6}$$

The relation between CCS and the collision strength is

$$\sigma_{fi} = \frac{\pi a_0^2}{k_i^2(2L_i+1)(2S_i+1)}\Omega_{fi}. \tag{7}$$

In the ionization process, the entire ionization amplitudes can be calculated by projecting $\psi_{l_1 l_2}^{LMS\Pi}$ to the continuum + continuum compound state as

$$F^S(\boldsymbol{k}_1, \boldsymbol{k}_2) = \sum_{l_1 l_2 LM} i^{-l_1-l_2} e^{i(\sigma_1+\sigma_2)} y_{l_1 l_2}^{LM}(\hat{\boldsymbol{k}}_1, \hat{\boldsymbol{k}}_2) f_{l_1 l_2}^{LMS}(k_1, k_2), \tag{8}$$

where

$$f_{l_1 l_2}^{LMS}(k_1,k_2) = \frac{2}{\sqrt{\pi}}\frac{\rho}{k_1 k_2} \times \int_0^{\pi/2}\left(\phi_1\phi_2\frac{\partial}{\partial\rho}\psi_{l_1 l_2}^{LMS} - \psi_{l_1 l_2}^{LMS}\frac{\partial}{\partial\rho}\phi_1\phi_2\right)d\alpha, \tag{9}$$

where $\rho = \sqrt{r_1^2 + r_2^2}$, $\alpha = \arctan(r_2/r_1)$, σ_1, σ_2 are the Coulomb phase shifts, ϕ_1, ϕ_2 are the Coulomb wavefunctions.[42–44] Finally, the triple differential cross section (TDCS) of the ionization process that contains the contributions of both the singlet and triplet two-electron states can be calculated as

$$\frac{d\sigma}{d\hat{\boldsymbol{k}}_1 d\hat{\boldsymbol{k}}_2 dE_2} = \frac{d\sigma^{S=0}}{d\hat{\boldsymbol{k}}_1 d\hat{\boldsymbol{k}}_2 dE_2} + \frac{d\sigma^{S=1}}{d\hat{\boldsymbol{k}}_1 d\hat{\boldsymbol{k}}_2 dE_2} = \frac{1}{4}\frac{k_1 k_2}{k_i}|F^{S=0}|^2 + \frac{3}{4}\frac{k_1 k_2}{k_i}|F^{S=1}|^2. \tag{10}$$

It is easy to understand that the above theory of ECS is independent on the interaction potentials; however, the initial and final states should be treated exactly. In the present work, we study the electron collision with a hydrogen atom in Debye plasmas, and the electron-proton and electron-electron interactions are screened. Specifically, the single electron Hamiltonian with the Debye-Hückel potential is

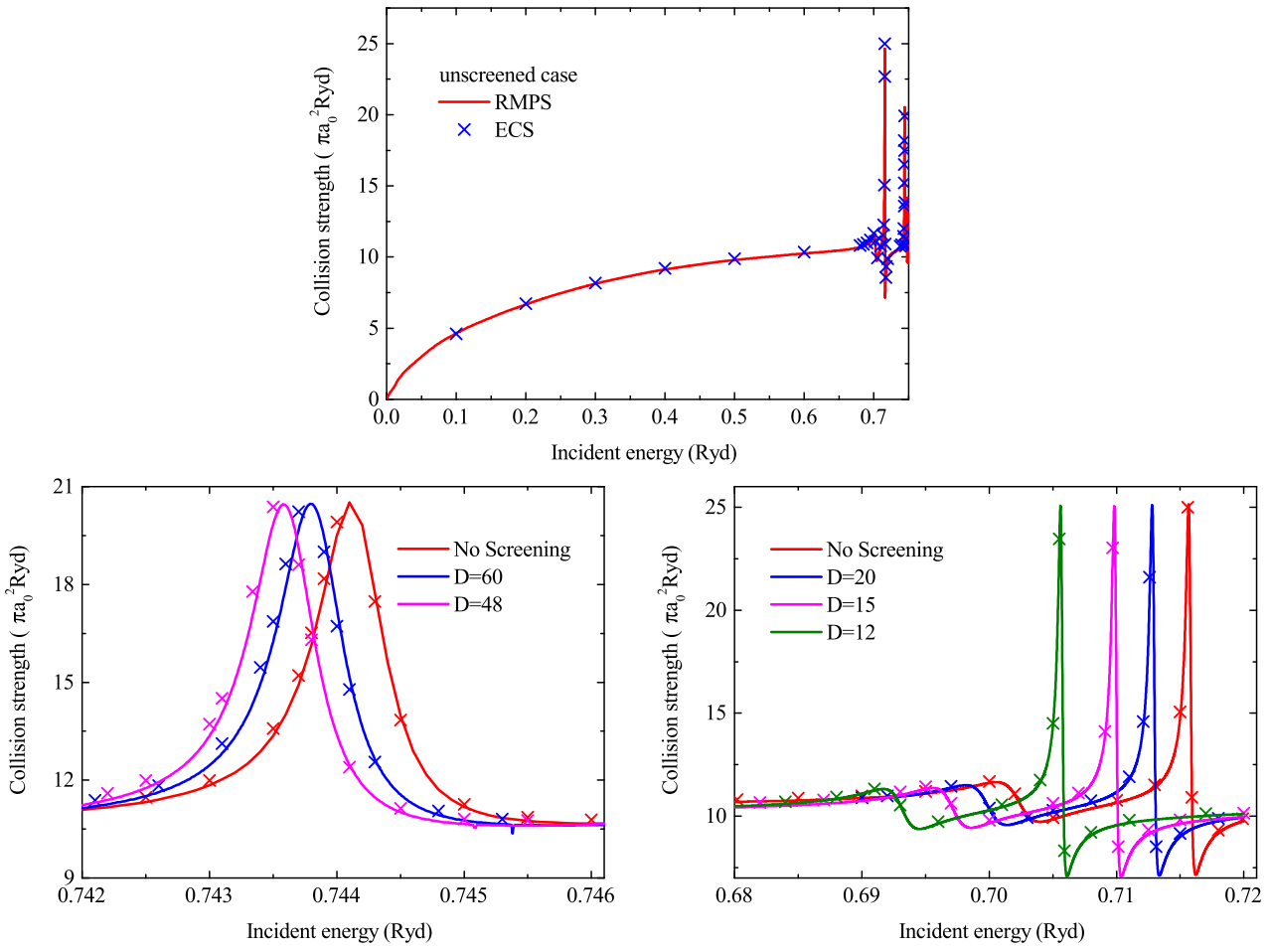

FIG. 1. 1*s*-1*s* elastic collision strengths. Lines: RMPS results;[34] crosses: present ECS results. Upper panel: unscreened case; lower panels: different screening lengths. (The screening length decreases from right to left.)

$$H_i = -\frac{1}{2}\nabla_i^2 - \frac{1}{r_i}\exp\left(-\frac{r_i}{D}\right), \tag{11}$$

and the electron-electron interaction is[34]

$$V_{12} = \frac{1}{r_{12}}\exp\left(-\frac{r_{12}}{D}\right), \tag{12}$$

where $r_{12} = |\mathbf{r}_1 - \mathbf{r}_2|$ is the inter-electron distance.

With the Hamiltonian of Eq. (11), the hydrogen bound orbitals $P_{n_i l_i}$ is obviously different from that of the pure Coulomb case, $P_{n_i l_i}$ in Eqs. (3) and (5) should be substituted by the screened bound orbitals; the continuum states of Hamiltonian Eq. (11) are not Coulomb wave functions anymore, and σ_i and ϕ_i $(i = 1, 2)$ should be replaced by the real continuum wave functions in the screened Coulomb field. In this work, the bound orbitals and the continuum wave functions in the screened field are numerically calculated by the RADIAL program.[52] The present ECS code is based on the modification of packages hex-ecs[43] and hex-db.[48]

III. RESULTS AND DISCUSSIONS

To verify the ECS packages for collisions in Debye plasmas, the elastic collision strengths ($1s$–$1s$) of electron-hydrogen atom collisions are calculated and compared with the published works[34] for different screening lengths. The calculated results for the unscreened case are shown in the upper panel of Fig. 1. They agree very well with the R-matrix method with pseudostates (RMPS) calculations of Zhang *et al*.[34] Peak structures contributed by the resonant states for different screening lengths are shown in the lower panels of Fig. 1. The figure shows that the present ECS calculations reproduce the RMPS results very well. Note that when calculating the very low energy impact excitations (e.g., $1s$–$2s$ excitation with the incident electron energy just above the $n = 2$ excitation threshold), the momentum of the outgoing free electron is small, large coordinate grid and many grid points are needed, and the ECS could meet numerical instabilities. In the following, TDCS of electron impact ionization of hydrogen in Debye plasmas are presented and discussed.

The calculations are performed in the conventional three different geometries of the coplanar equal-energy sharing kinematics. Fig. 2 shows the angles of the scattered and ionized electrons (or of two detectors) θ_1 and θ_2, respectively, relative to the direction of projectile electron. Let the angle clockwise be positive and vise versa. In the first geometry, the relative angle between the two detectors is kept constant (fixed $\theta_{12} = \theta_1 - \theta_2$), with the two detectors rotated together in the plane; the second one has a fixed angle θ_2 for one detector, with the other detector rotated in the plane; while in the last, so-called coplanar symmetric geometry, both detectors are rotated in the plane on either side of the incident electron beam with $\theta_2 = -\theta_1$.

The TDCS for the three coplanar equal-energy sharing geometries for the unscreened interaction case at 15.6 eV incident energy are shown in Fig. 3. Excellent agreement is found between the results of ECS theories and the experiment.[49,50]

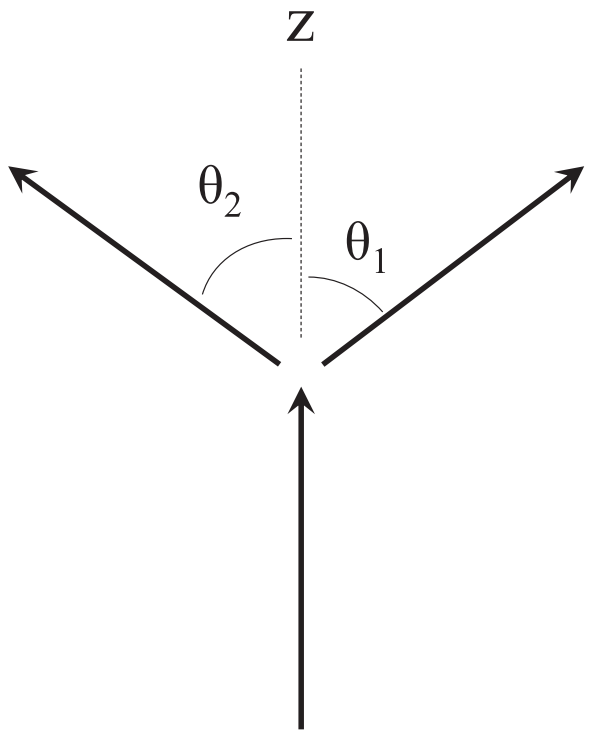

FIG. 2. Coplanar equal-energy-sharing kinematics for electron impact ionizations. Scattering happens at one plane, the direction of the incoming electron is chosen at z axis, the relative angles to z axis of the directions of the scattered, and ionized electrons are θ_1 and θ_2, respectively.

The present ECS results and the ECS results of Baertschy *et al*.[51] agree very well for all scattering angles, except for the small amplitude differences around the peaks of the structures. Note that the normalization of the experimental data could be incorrect.[51,53,54]

The TDCS in the screened interaction case for the coplanar geometry with fixed θ_{12} at 15.6 eV incident energy are shown in Fig. 4 as a function of the angle of scattered electron θ_1 for a number of θ_{12}-values between 180° and 80° and for screening lengths D between $50a_0$ and $5a_0$. The TDCS for the unscreened Coulomb potential for the same values of θ_{12} are also shown in this figure for comparison. The figure shows that the general structure of the TDCS in both the screened and unscreened cases is the same, indicating that the physical mechanisms involved in the collision dynamics are in both cases the same. The amplitudes of the peaks in the screened case, however, differ significantly from those in the unscreened case and their dependence on the screening length depends on the value of θ_{12}. Thus, for the cases of $\theta_{12} = 180°$ and 150°, the amplitudes of the peaks decrease as the screening length D decreases, while for the $\theta_{12} \geq 120°$ cases, they increase with decreasing D (this increase being stronger for the smaller θ_{12} values). It should be noted that the values of the dips in the cross section structures in the screened case are also different from those in the unscreened case, and their D dependence is different for the larger $(\theta_{12} \geq 120°)$ and smaller $(\theta_{12} \leq 100°)$ values of θ_{12} (cf. Fig. 4). The TDCS is symmetric with respect to the scattering angles $\theta_1 = \frac{1}{2}\theta_{12}$ and $\frac{1}{2}\theta_{12} + 180°$, where only the singlet contribution ($S = 0$) is retained in TDCS.[55] The pairs of peaks around the scattering angles $\theta_1 = \frac{1}{2}\theta_{12}$ and $\frac{1}{2}\theta_{12} + 180°$ are called forward peaks

and backward peaks, respectively, and have been discussed in several papers.[55,56] It should be noted in Fig. 4 that when the screening length varies, the positions of the forward and backward peaks are shifted with respect to those for the unscreened case. The angle differences $\Delta\theta_f$ and $\Delta\theta_b$ between the forward and backward peaks and $\theta_1 = \frac{1}{2}\theta_{12}$ and $\frac{1}{2}\theta_{12} + 180°$, respectively, for the different screening lengths D and θ_{12} angles extracted from Fig. 4 are shown in Fig. 5. When the screening length decreases, the forward peaks gradually shift towards the forward symmetric center $\theta_1 = \frac{1}{2}\theta_{12}$ ($\Delta\theta_f$ decreases), whereas the backward peaks shift oppositely towards the backward symmetric center $\frac{1}{2}\theta_{12} + 180°$ ($\Delta\theta_b$ increases). These properties are consistent with the changes of the peaks as θ_{12} increases for the unscreened case, where the

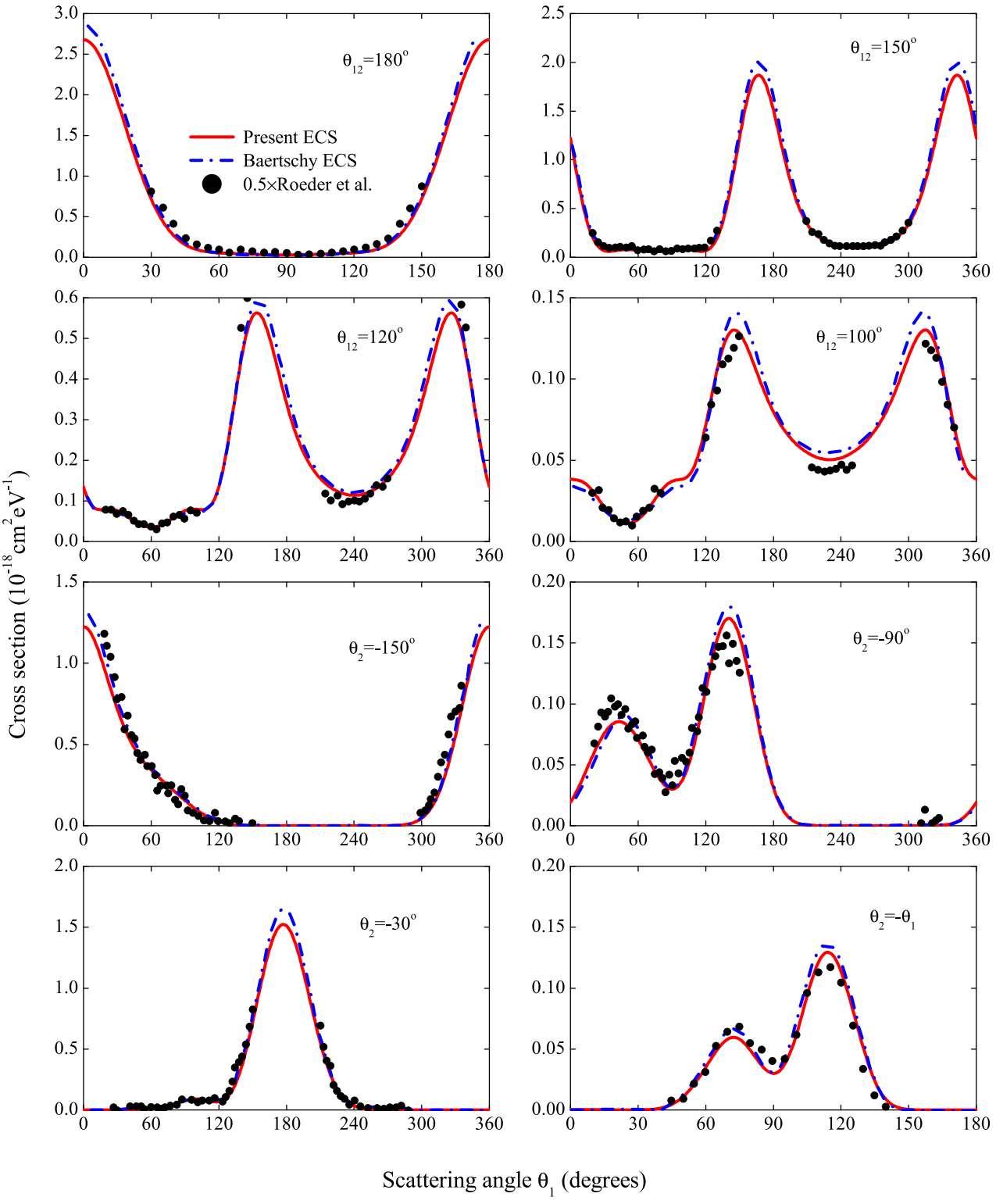

FIG. 3. Equal-energy-sharing TDCS at 15.6 eV incident energy for various coplanar geometries. Absolute experimental data (multiplied by 0.5)[49,50] and ECS calculations of Baertschy *et al.*[51] are compared.

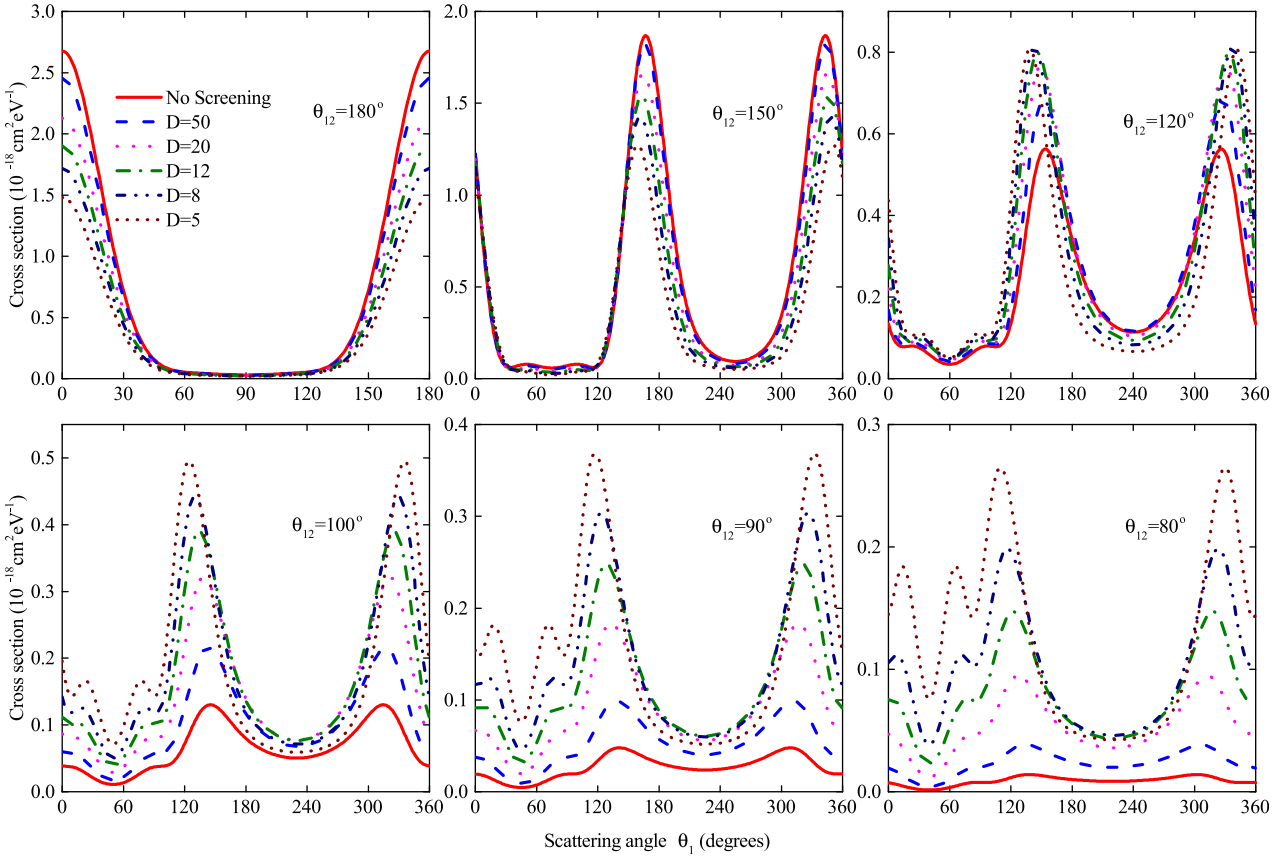

FIG. 4. Triple differential cross sections in Debye plasmas at incident energy of 15.6 eV in the coplanar equal-energy sharing geometry for different fixed angle θ_{12}.

electron-electron interaction decreases with the increasing of θ_{12}, as shown in Fig. 5.

The TDCS for the coplanar geometry with fixed θ_2 at 15.6 eV incident energy are shown in Fig. 6 for different screening lengths and for the unscreened case as a function of the angle θ_1. The contributions from the singlet and triplet states are also presented in the figure (the middle and the lowest sets of panels) to show their different contributions to the total cross section. Three typical cases with fixed $\theta_2 = -120°, -90°$, and $-60°$ are studied. The figure shows that the main features of the total TDCS in the unscreened case are the backward peak just below $\theta_1 = 180°$ and the forward peak around $\theta_1 = 0°$ (or 360°). The singlet and triplet contributions to these peaks are different: in the backward peak, the triplet contribution is negligible, while in the forward peak, they are roughly equal. Note that when θ_2 goes to $-180°$, the backward peak disappears and only the forward peak exists at $\theta_1 = 0°$; and when θ_2 goes to 0°, no forward peak exists anymore, the only backward peak is at $\theta_1 = 180°$. In the case of plasma screened Coulomb interactions, the general structure of TDCS remains roughly the same, but the amplitudes of the peaks and their positions change significantly. With the decrease in the screening length, the amplitude of the forward peak increases, whereas that of the backward peak decreases. The position of the forward peak shifts towards smaller θ_1 values (counter clockwise) while that of the backward peak shifts towards larger θ_1 values (clockwise). In the plasma, the singlet state continues to give the main contribution to the backward peak, while both singlet and triplet states contribute roughly equal to the forward peak, as in the unscreened case. Note that in the case of $\theta_2 = -60°$, the forward peak structure is very broad and shows a small shoulder (significant for $D = 12$ a.u.), which results from multi-peak structures contributed by the triplet state.

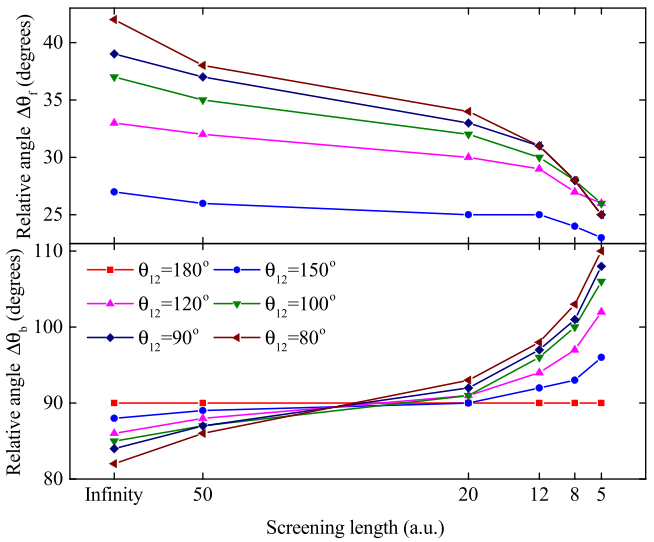

FIG. 5. Relative angles $\Delta\theta_f$ ($\Delta\theta_b$) between the forward peaks (backward peaks) to $\theta_1 = \frac{1}{2}\theta_{12}$ ($\theta_1 = \frac{1}{2}\theta_{12} + 180°$) with respect to the screening lengths.

Fig. 7 shows the TDCS for the coplanar symmetric geometry with $\theta_2 = -\theta_1$ at the incident energy of 15.6 eV

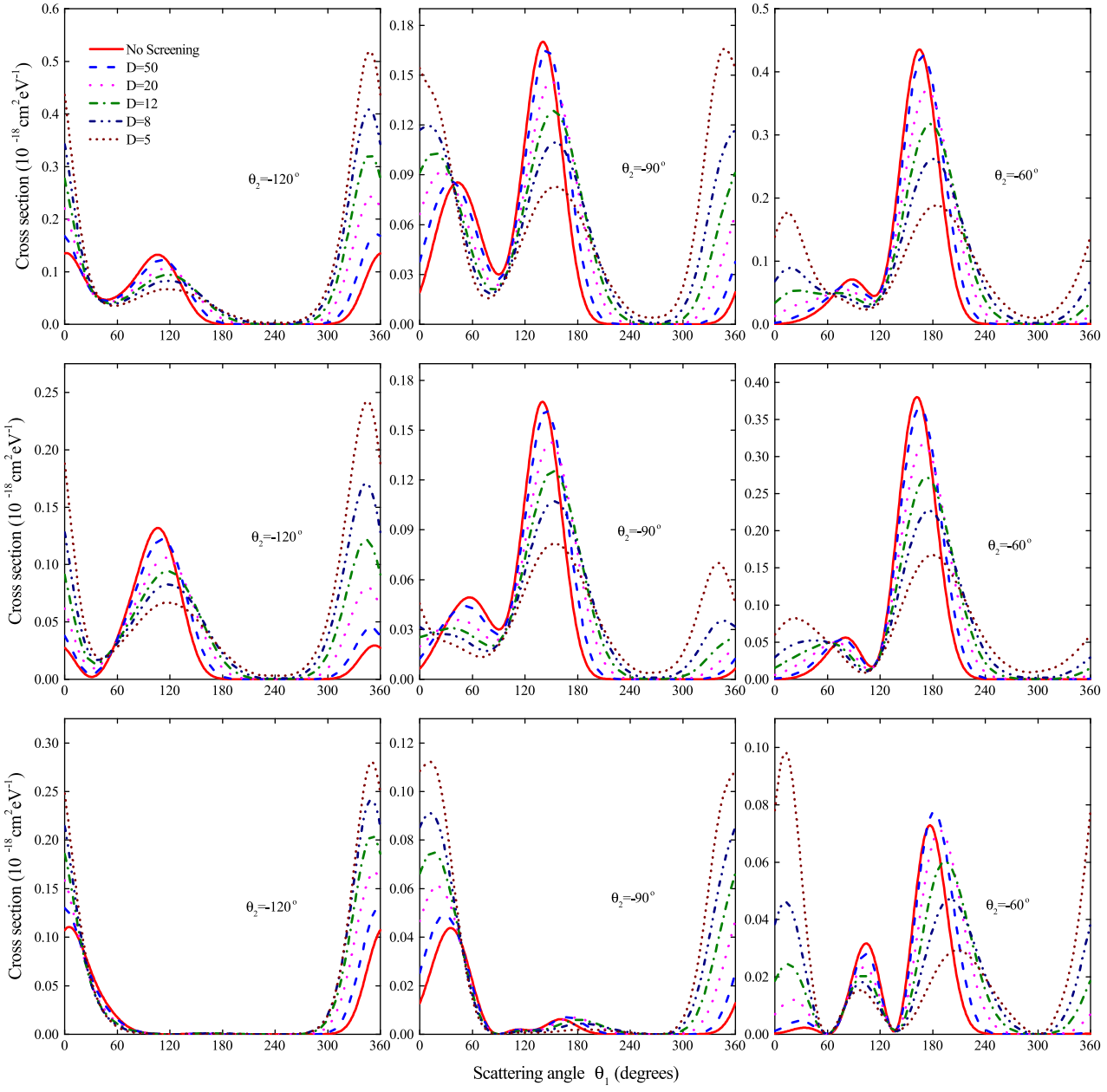

FIG. 6. Triple differential cross sections (upper panels) in Debye plasmas at incident energy of 15.6 eV in the coplanar equal-energy sharing geometry for different fixed angle θ_2. Middle and lower panels are the corresponding contributions from the singlet and triplet states, respectively.

for different screening lengths. Note that the triplet state cannot be formed in this geometry due to the Pauli exclusion principle, and only the singlet state contributes to the total TDCS. As shown in the figure, two peak structures dominate the TDCS: the backward peak is located at around 120° and the forward peak is below 90°. With the decrease in Debye screening length, the amplitude of the backward peak decreases and its position moves towards higher θ_1 values. The amplitude of the forward peak decreases with D decreasing until $D = 12a_0$ and then increases significantly with further decreasing of D. Its peak position shifts significantly towards the smaller scattering angles. For $D = 5a_0$, the forward peak becomes dominant (higher than the backward one) and even a third peak clearly shows up at 0°, which results from the complex softening of the Coulomb potentials.

The origin of the significant differences between the TDCS in the screened and unscreened Coulomb interaction cases is in the short-range character of the Debye-Hückel potential. As we mentioned in the Introduction, the energies of bound states in this potential decrease with decreasing screening length D, and their wave functions become increasingly more diffuse. The amplitude of electron radial density distribution of the 1s bound state of hydrogen atom in the screened case is significantly smaller than in the pure Coulomb case in the region near the proton (decreasing with decreasing D), but it becomes larger than the amplitude in the Coulomb case at large radial distances (increasing with decreasing D).[57,58] At the same time, the maximum of the distribution shifts to larger radial distances when D decreases. For a given (relatively small) continuum energy, the continuum wave function in the screened case is pushed

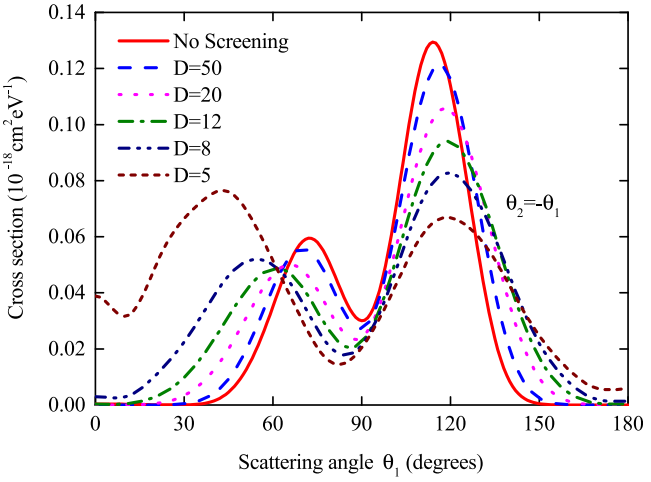

FIG. 7. Triple differential cross sections in Debye plasmas at incident energy of 15.6 eV in the symmetric coplanar equal-energy sharing geometry.

out further from the coordinate origin than in the unscreened case. With decreasing the screening length, the amplitude of the continuum wave function increases, while its frequency decreases.[17] These properties become more pronounced when the energy of the continuum electron decreases. The described differences between the bound state and continuum state electron wave functions involved in the ionization process generate the observed differences in the calculated TDCS. It should also be noted that due to the screening of electron-electron interaction, its role in the ionization dynamics should be reduced with respect to the unscreened case (e.g., the exchange effects).

IV. CONCLUSIONS

In this work, the exterior complex scaling method is employed to study scattering and ionization processes for electron hydrogen atom collisions in the Debye-Hückel potential for the first time. Our results for 1*s*–1*s* collision strengths for electron scattering with hydrogen atom in Debye plasmas show good agreements with previous calculations by the RMPS method and verify the method of calculations of this work. TDCS for electron impact ionization of hydrogen atom in Debye plasmas at an incident energy of 15.6 eV are studied and presented for three different coplanar equal-energy sharing geometries. The study shows that TDCS change significantly with the increasing screening effects. Different peak structures dominate the TDCS for different coplanar equal-energy-sharing geometries, and the evolutions of peak structures are studied in detail. The origin of the differences between the TDCS in the screened and unscreened Coulomb interaction cases is briefly discussed.

SUPPLEMENTARY MATERIAL

See supplementary material for the complete ASCII data for Figures 4, 6, and 7.

ACKNOWLEDGMENTS

The authors acknowledge Jakub Benda for his valuable instructions of the packages hex-ecs and hex-db. S. B. Zhang was partly supported by Shaanxi Normal University and the Organization Department of CCCPC. B. J. Ye was supported by the National Natural Science Foundation of China (Grants Nos. 11475165 and 11527811). J. G. Wang was supported by the National Basic Research Program of China (Grant No. 2013CB922200).

[1]J. P. Hansen and I. R. McDonald, *Theory of Simple Liquids* (Academic, London, 1986).
[2]D. Salzmann, *Atomic Physics in Hot Plasmas* (Oxford University Press, Oxford, 1998).
[3]M. S. Murillo and J. C. Weisheit, Phys. Rep. **302**, 1 (1998).
[4]H. Margenau and M. Lewis, Rev. Mod. Phys. **31**, 569 (1959).
[5]C. A. Rouse, Phys. Rev. **163**, 62 (1967).
[6]B. L. Whitten, N. F. Lane, and J. C. Weisheit, Phys. Rev. A **29**, 945 (1984).
[7]J. C. Weisheit, Adv. At. Mol. Phys. **25**, 101 (1989).
[8]Y. Leng, J. Goldhar, H. Griem, and R. W. Lee, Phys. Rev. E **52**, 4328 (1995).
[9]N. Woolsey, B. Hammel, C. Keane, C. Back, J. Moreno, J. Nash, A. Calisti, C. Mosse, R. Stamm, B. Talin *et al.*, Phys. Rev. E **57**, 4650 (1998).
[10]M. Nantel, G. Ma, S. Gu, C. Cote, J. Itatani, and D. Umstadter, Phys. Rev. Lett. **80**, 4442 (1998).
[11]A. Saemann, K. Eidmann, I. Golovkin, R. Mancini, E. Andersson, E. Förster, and K. Witte, Phys. Rev. Lett. **82**, 4843 (1999).
[12]M. Goto, R. Sakamoto, and S. Morita, Plasma Phys. Controlled Fusion **49**, 1163 (2007).
[13]H. Nguyen, M. Koenig, D. Benredjem, M. Caby, and G. Coulaud, Phys. Rev. A **33**, 1279 (1986).
[14]K. Scheibner, J. C. Weisheit, and N. F. Lane, Phys. Rev. A **35**, 1252 (1987).
[15]R. K. Janev, S. B. Zhang, and J. G. Wang, Matter Radiat. Extremes **1**, 237 (2016).
[16]G. Ecker and W. Kröll, Phys. Fluids **6**, 62 (1963).
[17]Y. Y. Qi, J. G. Wang, and R. K. Janev, Phys. Rev. A **80**, 063404 (2009).
[18]W. Kohn and C. Majumdar, Phys. Rev. **138**, A1617 (1965).
[19]L. Y. Xie, J. G. Wang, and R. K. Janev, Phys. Plasmas **21**, 063304 (2014).
[20]S. B. Zhang, J. G. Wang, R. K. Janev, Y. Z. Qu, and X. J. Chen, Phys. Rev. A **81**, 065402 (2010).
[21]L. Jiao and Y. Ho, Phys. Rev. A **87**, 052508 (2013).
[22]S. Kar and Y. Ho, Phys. Rev. A **79**, 062508 (2009).
[23]L. G. Jiao and Y. K. Ho, Int. J. Quantum Chem. **113**, 2569 (2013).
[24]S. Kar and Y. Ho, J. Phys. B **42**, 044007 (2009).
[25]L. Y. Xie, J. G. Wang, R. K. Janev, Y. Z. Qu, and C. Z. Dong, Euro. Phys. J. D **66**, 1 (2012).
[26]S. Kar and Y. K. Ho, Phys. Rev. A **86**, 014501 (2012).
[27]Y. Ho and S. Kar, Few-Body Syst. **53**, 437 (2012).
[28]Y. Ning, Z.-C. Yan, and Y. K. Ho, Phys. Plasmas **22**, 013302 (2015).
[29]S. Sahoo and Y. K. Ho, Phys. Plasmas **13**, 063301 (2006).
[30]Y. Y. Qi, Y. Wu, and J. G. Wang, Phys. Plasmas **16**, 033507 (2009).
[31]M. Das, B. K. Sahoo, and S. Pal, Phys. Rev. A **93**, 052513 (2016).
[32]A. Ghoshal and Y. K. Ho, Int. J. Quantum Chem. **111**, 4288 (2011).
[33]A. Ghoshal and Y. K. Ho, J. Phys. B **43**, 045203 (2010).
[34]S. B. Zhang, J. G. Wang, and R. K. Janev, Phys. Rev. A **81**, 032707 (2010).
[35]S. B. Zhang, J. G. Wang, and R. K. Janev, Phys. Rev. Lett. **104**, 023203 (2010).
[36]S. B. Zhang, J. G. Wang, R. K. Janev, and X. J. Chen, Phys. Rev. A **83**, 032724 (2011).
[37]K. A. Berrington, W. B. Eissner, and P. H. Norrington, Comput. Phys. Commun. **92**, 290 (1995).
[38]I. Bray and A. T. Stelbovics, Phys. Rev. Lett. **69**, 53 (1992).
[39]M. C. Zammit, D. V. Fursa, and I. Bray, Phys. Rev. A **82**, 052705 (2010).
[40]Y. Y. Qi, Y. Wu, J. G. Wang, and Y. Z. Qu, Phys. Plasmas **16**, 023502 (2009).
[41]Y. Y. Qi, L. N. Ning, J. G. Wang, and Y. Z. Qu, Phys. Plasmas **20**, 123301 (2013).
[42]P. L. Bartlett, J. Phys. B **39**, R379 (2006).
[43]J. Benda and K. Houfek, Comput. Phys. Commun. **185**, 2903 (2014).
[44]C. W. McCurdy, M. Baertschy, and T. N. Rescigno, J. Phys. B **37**, R137 (2004).

[45]T. N. Rescigno, M. Baertschy, W. A. Isaacs, and C. W. McCurdy, Science **286**, 2474 (1999).
[46]P. G. Burke, *R-Matrix Theory of Atomic Collisions: Application to Atomic, Molecular and Optical Processes* (Springer-Verlag, Heidelberg, 2011).
[47]I. Bray and A. T. Stelbovics, Phys. Rev. A **46**, 6995 (1992).
[48]J. Benda and K. Houfek, Comput. Phys. Commun. **185**, 2893 (2014).
[49]J. Röder, J. Rasch, K. Jung, C. T. Whelan, H. Ehrhardt, R. J. Allan, and H. R. J. Walters, Phys. Rev. A **53**, 225 (1996).
[50]J. Röder, H. Ehrhardt, C. Pan, A. F. Starace, I. Bray, and D. V. Fursa, Phys. Rev. Lett. **79**, 1666 (1997).
[51]M. Baertschy, T. N. Rescigno, and C. W. McCurdy, Phys. Rev. A **64**, 022709 (2001).
[52]F. Salvat, J. Fernández-Varea, and W. Williamson, Comput. Phys. Commun. **90**, 151 (1995).
[53]I. Bray, Phys. Rev. Lett. **89**, 273201 (2002).
[54]I. Bray, J. Phys. B **33**, 581 (2000).
[55]J. Berakdar and J. S. Briggs, J. Phys. B **29**, 2289 (1996).
[56]Z. Chen, Z. Ni, Q. Shi, and K. Xu, J. Phys. B **31**, 3803 (1998).
[57]F. Rogers, H. Graboske, Jr., and D. Harwood, Phys. Rev. A **1**, 1577 (1970).
[58]S. Zeng, L. Liu, J. Wang, and R. Janev, J. Phys. B **41**, 135202 (2008).